Dark photon dark matter exclusion limit using CB200 data

Date: 13.12.2024

V. Dabhi [a,*], J. Diehl [b], J. Egge [c], F. Hubaut [a], D. Leppla-Weber [c], P. Pralavorio [a]

[a]CPPM, Aix-Marseille Université, CNRS/IN2P3, Marseille, France
[b]Max-Planck-Institut für Physik, Garching, Germany
[c]Universität Hamburg, 22761 Hamburg, Germany

Abstract

In this work we present the results from the dark photon dark matter search performed at CERN using a prototype dielectric haloscope. The prototype uses 3 sapphire dielectric disks and a mirror to resonantly enhance the microwave signal induced by dark matter. Building on the data recorded for the axion search analysis inside the 1.6 T Morpurgo dipole magnet, this work presents 95% CL exclusion limit on the kinetic mixing of the dark photon dark matter down to 1.1×10^{-13} around the mass of 76.74 μ eV/c ^{2}. This limit surpasses previous constraints by almost 3 orders of magnitude, assuming a dark photon density ρ_χ in the galactic halo to be 0.3 GeV/cm^3 and unpolarized dark photons.

1 Introduction

To tackle the very pertinent question of dark matter in particle physics, the MAgnetized Disk and Mirror Axion eXperiment (MADMAX) collaboration uses the novel technology called dielectric haloscope [1]. It utilizes a metallic mirror and several dielectric disks to resonantly enhance (or "boost") the photon signal produced by dark matter candidates such as axions and dark photons. The first dark matter searches have already been accomplished by the collaboration, resulting in world best exclusion limit in the axion-photon coupling for axions and kinetic mixing angle for the dark photons around the mass of 80μeV [2] [3]. The very first physics result in the MADMAX collaboration was made by utilization of a dielectric haloscope prototype called open booster 300 (OB300) at University of Hamburg in December 2023 to search for dark photons.

In February-March 2024, the dielectric haloscope prototype called closed booster 200 (CB200) was employed to perform axion search inside 1.6 T magnetic field at MORPURGO magnet, CERN. It consists of an aluminium mirror and 3 sapphire disks of thickness 1 mm and diameter 200 mm, encased by an aluminium cylinder. A diagram of the CB200 prototype is seen in figure 1.

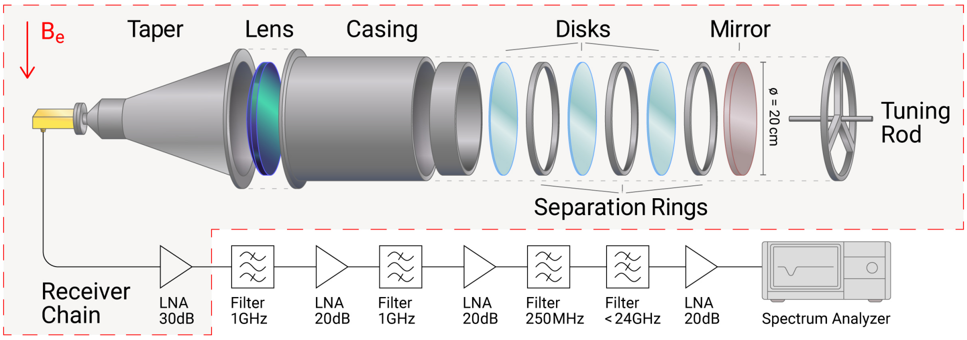

Figure 1: A schematic view of the prototype called CB200 along with the receiver chain [2]. The components inside the shaded region are exposed to the magnetic field.

The distances between the disks are controlled by 2 sets of separation rings. These distances determine the boosting response of the system, also called "boost factor". There is also a structure behind the mirror called tuning rod that can be used to push the mirror slightly and shift the frequency response of the system by O(10 MHz). Using a combination of the separation disks and the tuning rod, five different data runs were made for the axion search. Three physics-runs around 18.55 GHz and two around 19.21 GHz were performed.

The receiver system is connected at the end of the CB200 prototype as shown in figure 1, consisting of a series of low noise amplifiers (LNAs) and filters, and a Rohde & Schwarz FSW43 real-time spectrum analyser (SA). The SA streams time-domain data to a computer where it is Fourier transformed on GPUs with $\sim$ 0.11 s coherent integration length. The resulting power spectra are averaged in batches of 8047 single (raw) spectra, corresponding to roughly 15 min measurement time each. The receiver system has a bandwidth of $\sim$ 250MHz, which is approximately centred around the respective boost factor peak and provides negligible deadtime. A Y-factor method [4] is adopted to calibrate the output of the receiver system.

The aim of this work was to reproduce the results of the axion analysis performed on this data, and analyze the same data for dark photon signal.

2 Data Analysis

Boost factor distributions as a function of frequency are strongly correlated to the reflectivity measurements for the 5 different configurations of CB200 [2]. A one dimensional booster model is prepared in ADS software, which is fitted to the reflectivity measurements. Several parameters like the disk positions, disk thickness, dielectric loss, etc and their uncertainties are extracted from this fit. Losses due to three dimensional effects, such as tilts, are effectively included in the dielectric loss parameter.

The boost factor is reduced by a factor of 0.84 when we consider the overlap of the three dimensional field shape with the uniform axion current. An uncertainty of 12% is determined on this factor based on the field shape measurements using the bead pull method. Moreover, there are standing waves induced in between the booster and first Low noise amplifier (LNA) because the LNA impedance mismatch which modify the boost factor. These standing waves introduce a broadband frequency oscillation in the power spectra, depending on the distance between the LNA and the booster. This frequency behavior is modeled to calculate its influence on the boost factor. There is also a small uncertainty (less than 4%) in the boost factor, introduced by drifts in the frequency.

The boost factors are thus extracted for all five configurations. The maximum values for all is close to 2000, with uncertainties of 13 to 17 %.

The statistical analysis is the process of starting from the raw data and boost factor measurement to search for axion/dark photon dark matter signal and/or set an exclusion limit. For the MADMAX data taking of Feb-March 2024 using CB200 prototype [2], the raw data are power spectra measurements made in 15 min intervals. The auxiliary data consists of Temperature, Magnetic field, and vector network analyzer (VNA) measurements of booster power calibration.

The statistical analysis at MADMAX is based on the framework established by HAYSTAC collaboration [5]. The goal of the analysis is to combine individual power spectra in a way that maximizes the SNR, and then set an exclusion limit if no significant signal is observed. Measured power varies due to the time variations in the system. Therefore, a single measurement is taken over 15 min of integration time, which are reasonably constant. In a first analysis step, the baseline is removed and data is normalized so that axion signal would appear as a peak among Gaussian background noise. The relevant factors affecting the SNR are used later for rescaling the spectra.

After baseline removal, power excess in individual frequency bins in each spectrum can be considered as samples from a Gaussian distribution. The standard deviation of the Gaussian depends on the integration time of the spectra and the resolution bandwidth. It is crucial that the baseline removal process does not remove features with width comparable to the FWHM of the axion signal. This is achieved by selecting suitable parameter selection of the Savitzky-Golay (SG) filter used for baseline removal.

The analysis can be summarized in a few following steps [6]:

1. Cut away part of the data that is compromised by noise interference, malfunctioning of equipment, etc.

2. Use SG filter on the frequency domain data. The SG filter parameters should be chosen so that they do not significantly attenuate the potential axion signal, while also filtering the larger scale features in the data. SG filter window size of 1201 and order 4 is used in this particular analysis. Subtract the filtered spectra from the raw spectra and again divide the result by the filtered spectra. This process removes the baseline from raw power spectra and thus we obtain "Processed spectra". Each bin of a processed spectrum shows the power fluctuations of the data which are described by a Gaussian distribution.

3. Multiply each processed spectrum bin with the noise power and divide by the expected axion signal power (calculated using arbitrary value of $C_{a\gamma}$) in that bin to

obtain the “Rescaled spectra”. In a processed spectrum, there is uniform noise level in each bin whereas in a rescaled spectrum, the strength of the expected axion signal is uniform across bins. These rescaling factors insure that the expected power from an axion signal = 1 in each frequency bin. Here the expected axion power is calculated as [1]

$$P = 2.2 \times 10^{-27} \frac{W}{m^2} \beta^2 \left(\frac{B_e}{10\,T} \right)^2 C_{a\gamma}^2 \tag{1}$$

; where β^2 is the power boost factor, B_e is the external magnetic field, and $C_{a\gamma}^2$ is a constant denoting the strength of the axion-photon coupling with respect to the axion mass.

4. Construct a single “Combined spectrum” for the whole dataset by combining all the rescaled spectra. This is accomplished by taking a weighted sum of all bins belonging to the same frequency value. The weights are chosen using a maximum likelihood method that ensures the maximum SNR possible [5].

5. Correlate the adjacent bins of the combined spectrum with the expected axion line shape and obtain a “Grand spectrum”

6. After correcting for the effects of the SG filter on the SNR and the correlations in the grand spectrum, perform an axion search by looking for significant excess in the grand spectrum. If no significant excesses of unexplained origins are found, set an exclusion limit at 95% confidence level (corresponds to a value 1.645 sigma from mean in a Gaussian distribution) using [6]

$$|g_{a\gamma}|^{limit} = \sqrt{\frac{g_n/\sigma_f + 1.645}{R_n \cdot \eta_{SG}}} |g_{a\gamma}|^{ref} \tag{2}$$

; where $g_{a\gamma}$ is the axion-photon coupling, g_n is the grand spectrum, σ_f is the expected standard deviation of the grand spectrum, R_n is the expected signal strength for a given axion-photon coupling $g_{a\gamma}^{ref}$, and η_{SG} (0.92 in our case) is the attenuation of the SNR of the grand spectrum due to the application of SG filter.

3 Reproduction of axions analysis results

The primary aim of the data taking in February-March 2024 for the MADMAX collaboration was to search for axions. This was a very successful mission, leading to a world best exclusion limit for axions in the mass around 76 μeV and 79 μeV[2]. The work described in this document was partly conducted to independently reproduce of the results using the same analysis pipeline and software. This section includes the reproduction of all results related to the statistical analysis of the data from the paper [2]. The comparison is made separately for two frequency ranges hereafter called as “high frequency” and “low frequency". High frequency refers to the range from 19.17 GHz to 19.23 GHz while the low frequency refers to the range from 18.51 to 18.57 GHz. Together they form the analysis frequency range for this data.

The axions analysis is described in more detail in [6]. The MADbase and MADsearch software packages were used for the analysis and can be both found here: `https://gitlab.desy.de/madmax/`

Figure 2 shows the comparison of the grand spectra from the paper [2] (orange) and the reproduction (blue) as a function of the frequency. The bottom subplots show the difference between the two. It is shown that the difference between the reproduction and the original is very small (less than 0.04 absolute difference across the frequency).

Figure 3 shows the comparison of the total uncertainty on $g_{a\gamma}$ from the paper [2] (orange) and the reproduction (blue) as a function of the frequency. The bottom subplots show the relative difference between the two. It is shown that the relative difference between the reproduction and the original is very small (0.007% level).

Figure 4 shows the comparison of the observed 95% confidence level exclusion limit on the axion-photon coupling $|g_{a\gamma}|$ from the paper [2] (orange) and the reproduction (blue) as a function of the frequency. The bottom subplots show the relative difference between the two. It is shown that the relative difference between the reproduction and the original is small (less than 3%).

Figure 5 shows the comparison of the median expected 95% confidence level exclusion limit on the axion-photon coupling $|g_{a\gamma}|$ from the paper [2] (orange) and the reproduction (blue) as a function of the frequency. The bottom subplots show the difference between the two. It is shown that the relative difference between the reproduction and the original is small (0.005 % level).

The small discrepancies in the grand spectrum and the observed 95% confidence level exclusion limit can be ascribed to small computational differences in the analysis code, but overall all results of [2] are very well reproduced.

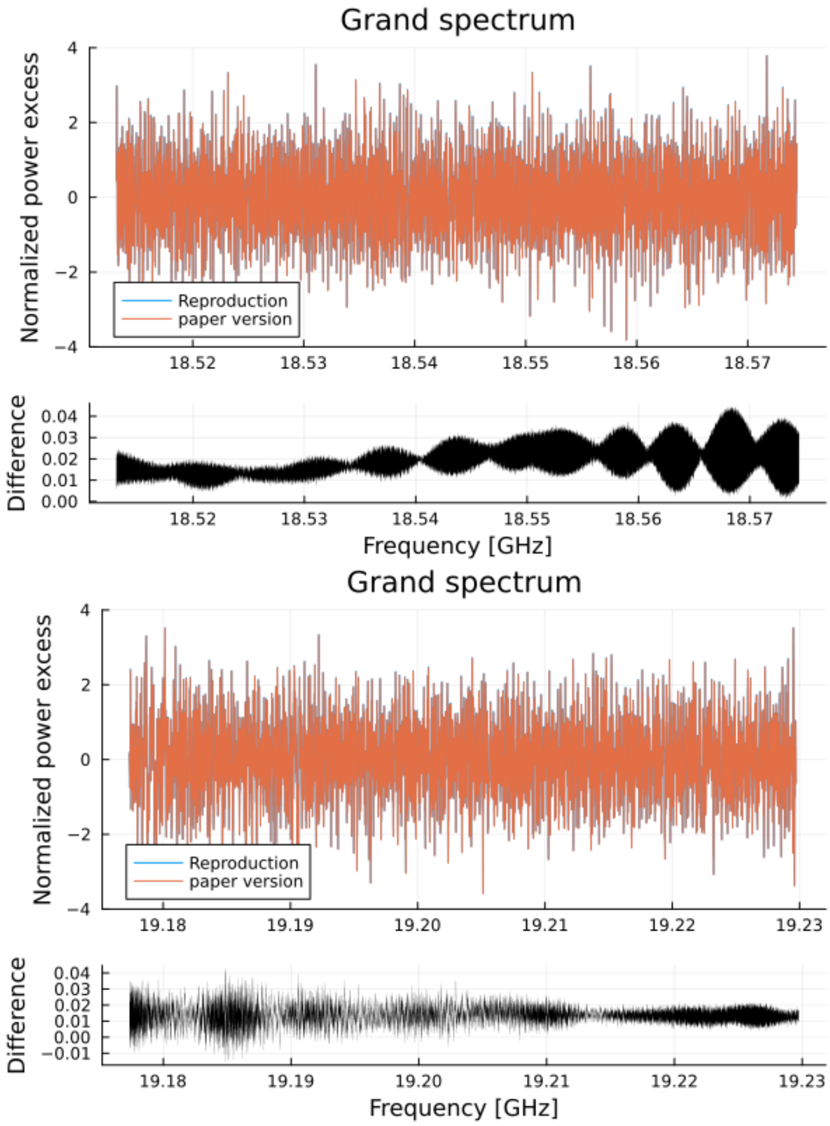

Figure 2: Grand spectrum comparison for the low and high mass ranges. The data from the paper is shown in orange while the reproduction is shown in blue. The bottom plots show the difference between the two.

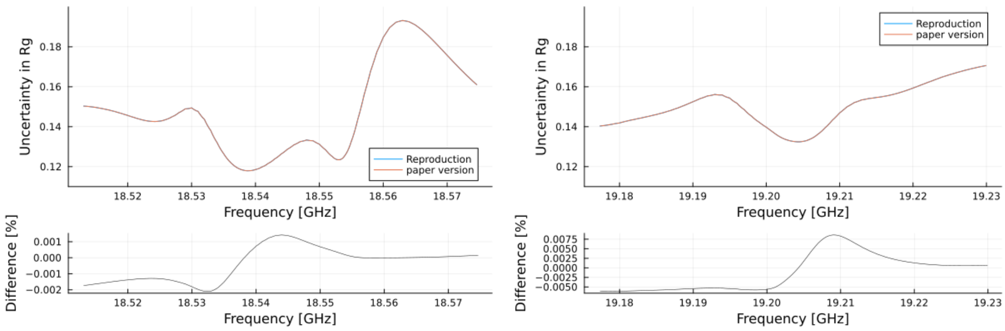

Figure 3: The uncertainty in the grand spectrum for the low and high mass ranges. The data from the paper is shown in orange while the reproduction is shown in blue.

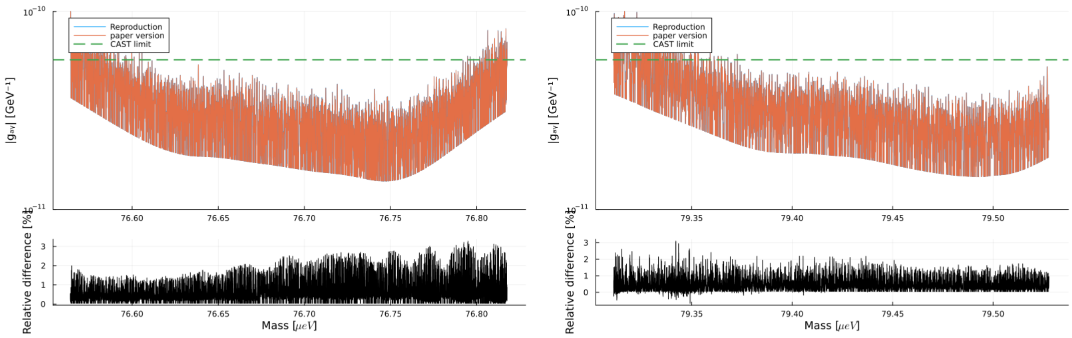

Figure 4: The observed 95% CL limit on axion-photon coupling for the low and high mass ranges. The data from the paper is shown in orange while the reproduction is shown in blue.

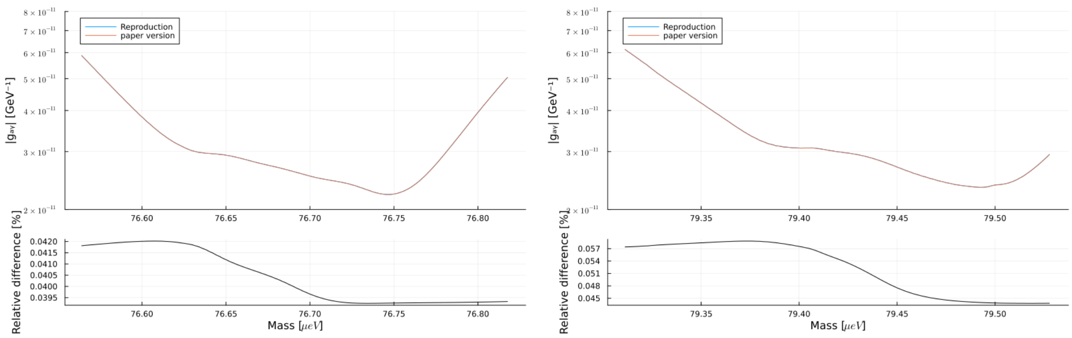

Figure 5: The median expected 95% CL limit on axion-photon coupling for the low and high mass ranges. The data from the paper is shown in orange while the reproduction is shown in blue.

4 Dark photon run analysis

The analysis for the dark photon run follows the same steps and software as that of the axions analysis, except at few places. The ALPs analysis was done excluding many timestamps (1 timestamp = raw data integrated for 15 minutes) because of low magnetic field availability. Since dark photons do not need the magnetic field to produce a signal, all data (1602 timestamps in total) has been included in this analysis. The first is the expected power in a given bin of a spectrum; which is different for the axions and the dark photon (step 3 of section 1) [3]:

$$P_0 = \chi^2 c \rho_\chi A \beta^2 \alpha_{pol}^2 \tag{3}$$

; where P_0 is the signal power, χ is the kinetic mixing angle for dark photon, c is the speed of light, ρ_χ is the dark photon density, A is the surface area, β^2 is the power boost factor, and α_{pol}^2 is the polarization factor (average fraction of dark photons that the experiment is sensitive to).

The second place is the procedure to calculate the exclusion limit from the grand spectrum, where we calculate an exclusion limit for the kinetic mixing for the dark photon, and axion-photon coupling for the axions (step 6 in section 1):

$$|\chi|^{limit} = \sqrt{\frac{g_n/\sigma_f + 1.645}{R_n \cdot \eta_{SG}}} |\chi|^{ref} \tag{4}$$

; where χ is the kinetic mixing angle for dark photon, g_n is the grand spectrum, σ_f is the expected standard deviation, R_n is the expected signal strength for a given dark photon kinetic mixing, and η_{SG} is the attenuation of the SNR of the grand spectrum due to the application of SG filter.

These changes have been adapted in the MADsearch package branch called 'darkphoton'.

For the dark photon analysis, we use the same boost factor values that are calculated for the ALPs analysis. The justification for this step can be given using using the reciprocity approach as described in [7] and [8]. The reciprocity approach for axions and dark photons are fully analogous to each other by converting between the axion current density J_a and the dark photon current density J_χ. The dark photon signal power is given by [8]

$$P_{sig,\chi} \propto \left| \int_{V_a} dV \boldsymbol{E}_R \cdot \boldsymbol{E}_\chi \right|^2 \tag{5}$$

, where V_a is the detector conversion volume, E_R is the reflection induced field, and E_χ is the dark photon electric field. The polarization of the field E_χ is unknown. Here we assume that it has random polarization. Therefore, we need an average over all possible polarizations for the integral. The signal power can now be rewritten as

$$P_{sig,\chi} \propto \alpha_{pol}^2 \left| \int_{V_a} dV E_R \langle |E_\chi| \rangle_{pol} \right|^2 \tag{6}$$

, where factor $\alpha_{pol}^2 = 1/3$ applies to experiments sensitive to only one polarization of the electric field. Having accounted for the polarization of the dark photons in this manner, the dark photon signal power can be treated just like axions. Therefore we use the boost factor distributions obtained for the axion case and apply it directly to dark photon analysis.

5 Dark photon exclusion limit

As in the axion analysis, no signals of unknown origins are found in the grand spectrum. A 95% confidence level exclusion limit is set on the dark matter dark photon kinetic mixing angle χ using the same procedure as the axion analysis [2]. The systematics for the limit are also included in the same way as the axion analysis. Figure 6 shows the observed limit along with the median expected limit and 16% and 84 % quantiles limit.

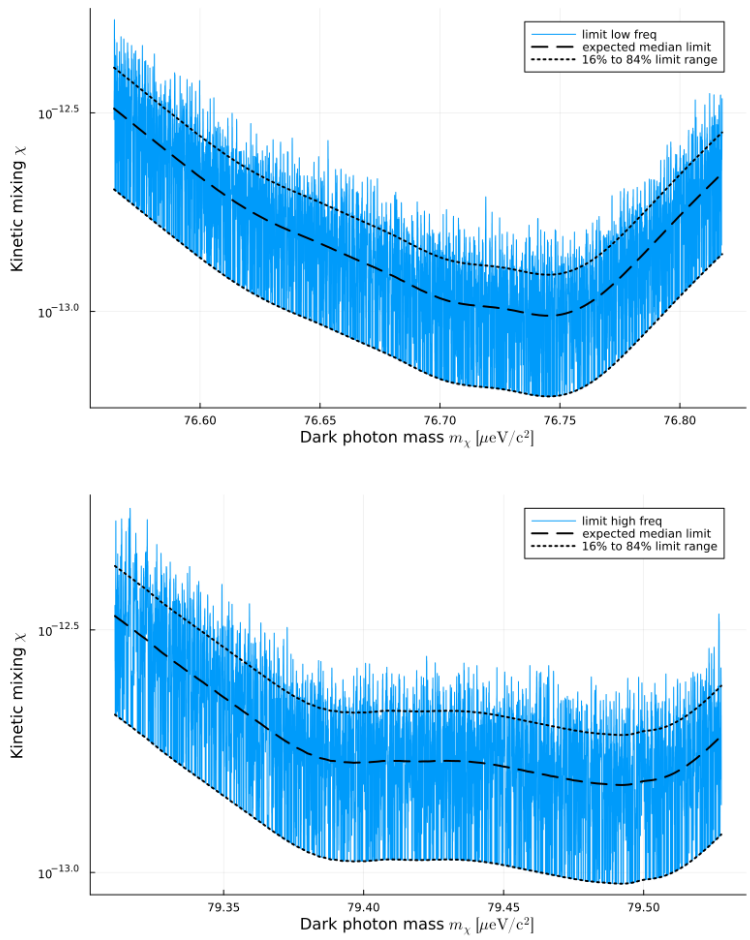

Figure 6: The observed 95% CL limit (in blue) on kinetic mixing of dark photons for the low and high frequency datasets. The black dashed line shows the median expected limit and the dotted lines show the 16% and 84 % quantiles.

This exclusion limit is further smoothened by marginalizing over 210 neighboring bins together using the approach described in [9]. This smoothening is also used in the dark photon analysis of [3]. The process involves generating a random distribution for each bin with the observed excess as the mean and the standard deviation of 1. 200 samples are generated from this random distribution, and the negative values are all set to zero. These 200 randomly generated samples for 210 bins are all sorted and the 95% confidence limit is determined by the 95 percentile value from the top. This rebinned upper limit is shown in figure 7 for the low mass and high mass regime with 0.19 MHz bins.

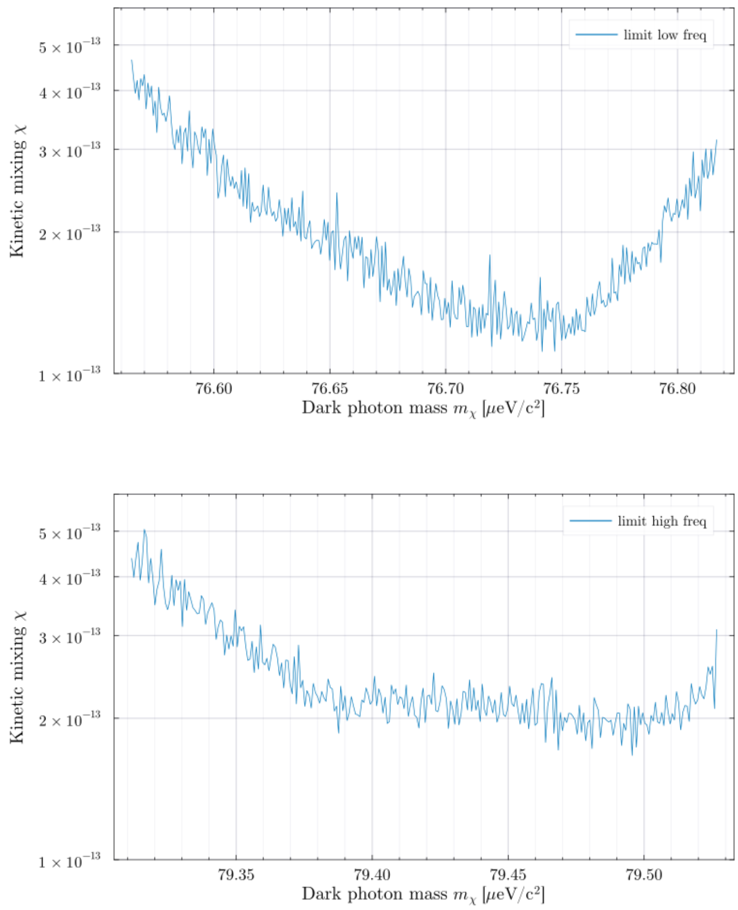

Figure 7: The observed 95% CL rebinned limit on kinetic mixing of dark photons for the low and high frequency datasets.

6 Conclusion

The 95% CL limit on the dark photon kinetic mixing angle χ is shown in figure 8. Unpolarized dark photon dark matter ($\rho_\chi = 0.3$ GeV/cm^3) with $\chi > 5.0 \times 10^{-13}$ can be excluded for masses between 76.56 to 76.82 μeV/c^2 and 79.31 to 79.53 μeV/c^2. We have improved existing limits by up to almost three orders of magnitude with a peak sensitivity of $\chi = 1.1 \times 10^{-13}$ at the mass 76.74 μeV/c^2. Compared to the previous broadband dark photon search using OB300 prototype, this work shows the validity of narrow band search with more resonant configuration and smaller CB200 prototype.

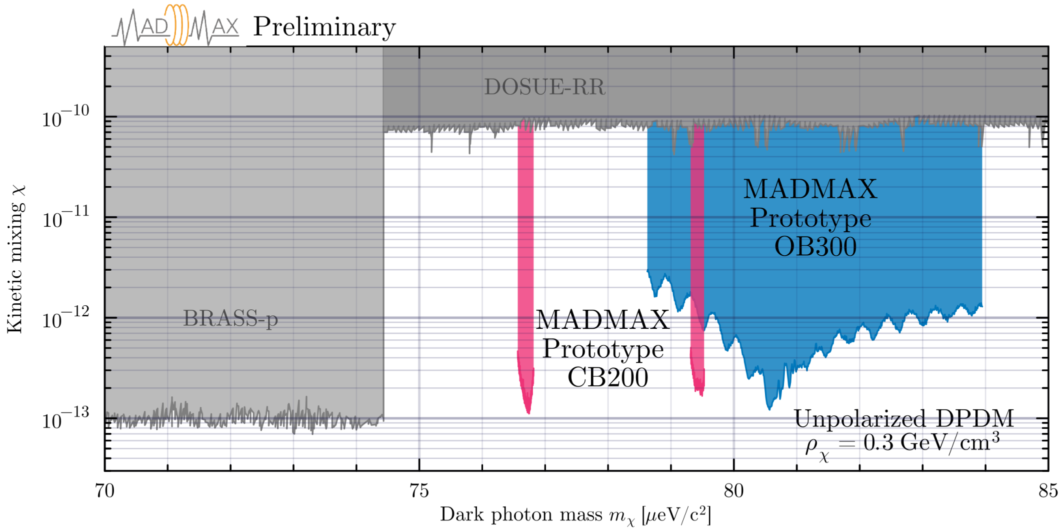

Figure 8: 95% CL upper limit on dark matter dark photon kinetic mixing angle χ obtained with this work. These limits (in red) are compared to the dish antenna experiments DOSUE-rr [10], BRASS-p [11] and another MADMAX prototype used in broadband regime (in blue) [3]. Dark photons are assumed to be unpolarized. The local dark matter density is assumed to be 0.3 GeV/cm^3.

References

[1] P. Brun et al. *A new experimental approach to probe QCD axion dark matter in the mass range above 40 μeV*. *Eur. Phys. J. C*, 79(3):186, 2019, 1901.07401.

[2] B. Ary dos Santos Garcia et al. *First search for axion dark matter with a Madmax prototype*, 9 2024, 2409.11777.

[3] J. Egge et al. *First search for dark photon dark matter with a MADMAX prototype*, 8 2024, 2408.02368.

[4] D.M. Pozar. *Microwave Engineering*. Wiley, 2012.

[5] B. M. Brubaker, L. Zhong, S. K. Lamoreaux, K. W. Lehnert, and K. A. van Bibber. *HAYSTAC axion search analysis procedure*. *Phys. Rev. D*, 96(12):123008, 2017, 1706.08388.

[6] J. H. B. Diehl. *Statistical Methods for a First MADMAX Axion Dark Matter Search and Beyond*. PhD thesis, TUM School of Natural Sciences, 2024.

[7] J. Egge. *Axion haloscope signal power from reciprocity*. *JCAP*, 04:064, 2023, 2211.11503.

[8] J. Egge. *The Sensitivity of Dielectric Haloscopes to Dark Matter Axions and Dark Photons*. PhD thesis, Universit

[9] C. Bartram et al. *Axion dark matter experiment: Run 1B analysis details*. *Phys. Rev. D*, 103(3):032002, 2021, 2010.06183.

[10] S. Kotaka et al. *Search for Dark Photon Dark Matter in the Mass Range 74–110 μeV with a Cryogenic Millimeter-Wave Receiver*. *Phys. Rev. Lett.*, 130(7):071805, 2023, 2205.03679.

[11] F. Bajjali et al. *First results from BRASS-p broadband searches for hidden photon dark matter*. *JCAP*, 08:077, 2023, 2306.05934.

7 Appendix: Expected sensitivity

Before performing the statistical analysis of the search of the dark photons, a sensitivity calculation was made to estimate its competitiveness compared to existing constraints in this mass range set by the DOSUE-rr experiment [10]. One of the low frequency data run called “29_overnight” and a high frequency data run called “23_weekend” were used to make this calculation, as it is harder to calculate the sensitivity combining all 5 data runs. For a dielectric haloscope, the sensitivity on kinetic mixing angle for the dark photon is given as [3]

$$\chi = 1.03 \times 10^{-13} \left(\frac{640}{\beta^2}\right)^{1/2} \left(\frac{707\ \mathrm{cm}^2}{A}\right)^{1/2} \left(\frac{T_{sys}}{240\ \mathrm{K}}\right)^{1/2} \left(\frac{11.7\ \mathrm{days}}{t}\right)^{1/4} \left(\frac{\mathrm{SNR}}{5}\right)^{1/2} \left(\frac{0.3\ \mathrm{GeV/cm}^3}{\rho_\chi}\right)^{1/2} \left(\frac{\Delta\nu_\chi}{20\mathrm{kHz}}\right)^{1/4} \tag{7}$$

; where β^2 is the boost factor, A is the surface area, T_{sys} is the system temperature, t is the data integration time, ρ_χ is the dark photon density in the galaxy halo, and $\Delta\nu_\chi$ is the width of the dark photon signal in frequency.

In table 1, the sensitivities of a data run from high and low frequency is calculated at the frequency of the booster peak using equation 7. The estimated sensitivity is given in the last row of the table.

Data run	23_weekend	29_overnight
Frequency	19.215 GHz	18.543 GHz
β^2	2042	2062
Area	$\pi \times (9.8)^2$	$\pi \times (9.8)^2$
T_{sys}	600	383
Integration time	2.52 days	3.07 days
SNR	5	5
ρ_χ	0.3 GeV/cm ^{3}	0.3 GeV/cm ^{3}
$\Delta\nu_\chi$	20 kHz	20 kHz
χ eq. 7	2.05×10^{-13}	1.55×10^{-13}

Table 1: Sensitivity calculation for the 23_weekend run from the high frequency dataset and 29_overnight run from low frequency dataset using equation 7.